Applied Catalysis B: Environmental 111–112 (2012) 38–45

Contents lists available at SciVerse ScienceDirect

Applied Catalysis B: Environmental

journal homepage: www.elsevier.com/locate/apcatb

Synthesis of mesoporous nitrogen–tungsten co-doped TiO_2 photocatalysts with high visible light activity

Sapanbir S. Thind, Guosheng Wu, Aicheng Chen*

Department of Chemistry, Lakehead University, 955 Oliver Road, Thunder Bay, ON P7B 5E1, Canada

ARTICLE INFO

Article history:
Received 6 June 2011
Received in revised form 7 September 2011
Accepted 15 September 2011
Available online 22 September 2011

Keywords:
Photocatalysis
Mesoporous
TiO_2
N,W co-doping
Visible light activity

ABSTRACT

Mesoporous N,W co-doped TiO_2 photocatalysts that contained various percentages of atomic tungsten dopant levels were synthesized by a facile solution combustion method which utilized urea as a nitrogen source and sodium tungstate as a tungsten source. The prepared samples were characterized by X-ray diffraction (XRD), transmission electron microscope (TEM), N_2 physisorption, UV–vis absorbance spectroscopy, and X-ray photoelectron spectroscopy (XPS). The results reveal that the synthesized N and W co-doped TiO_2 nanomaterials have high surface areas and mesoporous structures. In addition, the co-doping significantly narrows the band gap (~2.7 eV) that is responsible for the high visible light response of these samples in comparison to that of pure anatase TiO_2 (~3.2 eV). The photocatalytic activity of the prepared samples was evaluated on the basis of the photodegradation rate of Rhodamine B under visible light ($\lambda > 420$). It was found that the mesoporous N,W co-doped TiO_2 nanomaterials fabricated in this study exhibited high visible light activity. This significant improvement in photocatalytic activity may be attributed to the synergistic effect of the red shift in absorption combined with a high surface area.

1. Introduction

The extensive use of dyes in the textile, cosmetic and plastics industries and their subsequent release via wastewater into the ecosystem is one of the major sources of environmental pollution [1,2]. Due to the high resistivity of these modern dyes toward chemical and microbiological degradation, they are becoming an increasing threat to aquatic life as a result of their tendency to cause aesthetic pollution and eutrophication [3,4]. Dyes containing N atoms can undergo reductive anaerobic degradation to produce cancer causing aromatic amines [5]. Hence, it is critical that these dyes undergo sufficient degradation prior to their release into wastewaters in order to protect fragile ecosystems. Heterogeneous photocatalysis has demonstrated superiority toward the abatement of organic pollutants over conventional methods (e.g., occulation, reverse osmosis, activated carbon adsorption, ozonization and chemical oxidation technologies), which have inherent problems in the complete removal of color and for the potential generation of secondary pollution [6]. In recent years, a great effort has been placed on the development of clean and inexpensive heterogeneous photocatalysts for the elimination of myriad pollutants from water.

TiO_2 is one of the most intensely investigated semiconductor photocatalysts which may be utilized for the environmentally compatible treatment of inorganic and organic pollutants due to its chemical inertness, high efficiency, non-toxicity and low cost [7,8]. However, a significant constraint that prevents its pervasive implementation is that the TiO_2 based photochemical process may only be initiated by UV light, due to its large energy band gap (~3.2 for anatase) [9]. Unmodified TiO_2 photocatalysts show negligible response to visible light (which constitutes a significant portion of natural sunlight). The modification of the electronic structure of TiO_2 based materials is thus required to shift the absorption edge to the visible region in order to enhance and expand the utilization of renewable solar energy. A common approach in shifting the absorption edge of TiO_2 to the visible region is to modify its electronic structure by substituting the oxygen in the lattice with anionic dopants such an N, C, S and halogen atoms [10–12]. Among these, N stands out as the most promising candidate due to its comparable ionic radius, which is close to that of O such that N2p states may effectively merge with O2p states. This modifies the electronic structure of the valance band, which facilitates the transport of charge carriers. Nonmetal doping also induces oxygen vacancies, which have a significant influence on catalytic activity [13]. Asahi et al. [14] prepared N doped TiO_2 via the sputtering method and showed absorption in the visible region due to the formation of the O–Ti–N bond. This hypothesis was supported by the presence of the N1s peak at 397 eV that was observed during the XPS analysis. Following this discovery, it was confirmed by a

* Corresponding author. Tel.: +1 807 3438318; fax: +1 807 3467775.
E-mail address: aicheng.chen@lakeheadu.ca (A. Chen).

0926-3373/$ – see front matter © 2011 Elsevier B.V. All rights reserved.
doi:10.1016/j.apcatb.2011.09.016

number of researchers that the N1s peak at 397 eV is responsible for the visible light response, as N substitutes for the O atoms in the lattice structure of TiO_2, causing a modification in its electronic structure [15]. Although N-doped TiO_2 exhibits good visible light induced photocatalytic activity, electron–hole recombination remains a major obstacle that blocks the effective use of TiO_2 photocatalysts, which are doped with only non-metals [16,17]. This deficiency has spurred the development of co-doped TiO_2, which may involve the combination of non-metal and metal elements or two different non-metal elements. Due to the synergistic effect of both dopants, co-doped TiO_2 show greater visible response than single doped TiO_2 [18,19]. However, very few studies of N,W co-doped TiO_2 photocatalysts have been reported in the literature. Kubacka et al. employed a microemulsion method to fabricate N,W co-doped TiO_2 with over 10% of W [20,21]. Dai and co-workers used a slow hydrolysis approach in an ice-water bath to synthesize twist-like helix tungsten–nitrogen-co-doped titania [22]. A two-step method has also been reported, where N-doped TiO_2 nanoparticles were fabricated first using a sol–gel method, and followed by either mechanical alloying with W-doped TiO_2 nanoparticles [23] or dispersing the N-doped TiO_2 powders in a dilute ammonia solution containing tungstic acid [24].

In the present work, a novel and facile solution combustion synthesis method was developed and employed to prepare N,W co-doped TiO_2 nanomaterials that contained various percentages of atomic tungsten dopant levels. The one-step solution combustion method is much less time consuming compared to the sol–gel method and the microemulsion method; and it does not involve any expensive or complicated instruments. Our experimental results show that the synthesized N,W co-doped TiO_2 exhibit the photocatalytic active anatase phase exclusively, with a very high surface area and mesoporous structure consisting of particles of between 8–12 nm in size. The fabricated N,W co-doped TiO_2 nanomaterials show marvelous photocatalytic activity under visible light irradiation.

2. Experimental

2.1. Photocatalyst synthesis

To prepare the mesoporous N-doped or N,W co-doped TiO_2, commercially available titanium (IV) isopropoxide (TTIP) (Sigma–Aldrich, 97%,) was used as a Ti precursor, urea (Sigma–Aldrich, ≥99%) as a nitrogen source and sodium tungstate ($Na_2WO_4{\cdot}2H_2O$, Sigma–Aldrich) as a tungsten source, ethanol as a solvent and acetic acid as an inhibitor to the hydrolysis of the organic precursor. 2 ml of TTIP was added dropwise to a mixture of 20 ml of ethanol and 0.5 ml of acetic acid under vigorous stirring for 30 min. To obtain an equivalent composition of N in all samples, 5 g of urea and a predetermined amount of 0.1 M Na_2WO_4, based on the target composition of W, were added. Initially, the mixed solution was heated on a hot plate, and subsequently, to facilitate the combustion reaction, the solution was transferred to a preheated (300 °C) furnace. Finally, the synthesized powder was calcinated at 450 °C for 3 h.

2.2. Characterization techniques

The crystalline phase of the synthesized samples was obtained by X-ray diffraction (Phillips PW 1050-3710 Diffractometer with Cu Kα radiation (λ = 1.5406 Å). For the determination of the Brunauer–Emmett–Teller (BET) surface area of the samples, N_2 gas adsorption/desorption studies at liquid nitrogen temperature (77 K) were conducted utilizing a Quantachrome Nova 2200 surface area and pore size analyzer. The samples were initially degassed at 400 °C for 3 h under vacuum. Transmission electron microscopy (JEOL 2010) analysis was performed in order to determine the surface morphology and particle size of the samples. The UV–vis absorbance spectrum was obtained using a UV–vis spectrophotometer (Varian, Cary 5E). The surface composition was examined by X-ray photoelectron spectroscopy (Omicron EA-125 energy analyzer and a multi-channel detector). All binding energies reported in this work were corrected using the C1s peak at 284.5 eV as an internal standard. The broad N1s region of the sample was fitted using XPSPEAK41 software.

2.3. Photocatalytic activity measurements

The photocatalytic activity of as synthesized powders and Degussa P25 was evaluated by measuring the photodegradation of Rhodamine B (organic dye pollutant) under visible light. The reactor is a cylindrical pyrex vessel having internal diameter of 4 cm and 4.5 cm internal height and is open to the air. In a general experiment, 20 mg of the photocatalyst was suspended in 20 ml of 25 μM aqueous solution of Rh B. The depth of the solution in the reactor was ~2 cm. The distance between the surface of the reactor and the light source was kept at 3 cm. The Rhodamine solution was prepared using pure water (18.2 MΩ cm) obtained from a NANOpure® Diamond™ UV ultrapure water purification system. The reaction mixture was sonicated for 30 min in the absence of light in order to obtain a homogeneous suspension and to achieve an adsorption–desorption equilibrium. The light source used in this study consisted of an Oriel system including a 300 W xenon arc lamp. The lamp was allowed to warm up for half an hour before testing. For visible light irradiance, the source light was passed through an optical filter (Edmund Optical Co. GG420), which cut off wavelengths of below 420 nm. Infrared light was removed by a water filter. The wavelength range of the resulting light was between 420 and 700 nm with the intensity of ~2.50 mW cm^{-2} measured by a Cole-Palmer Instrument (Radiometer Series 9811) at the point where the light entered the reactor. Samples were collected from the reaction mixture at 20 min increments. The samples were centrifuged (Thermo Electron Co., Sorvall Biofuge Stratos Ccentrifuge) to remove particles from the solution and this particle free solution was used to measure the degradation of Rh B using a UV–vis spectrometer (Varian, Cary 50). The solution and the centrifuged particles were then added back to the reactor.

3. Results and discussion

3.1. XRD analysis

The XRD patterns of the synthesized powders are presented in Fig. 1. Among the anatase, rutile and brookite phases of TiO_2 only the diffraction peaks of the higher photocatalytic active anatase phase was observed in all samples. Additional peaks from WO_3 due to inhomogeneous doping or from any impurities were not observed, which signifies that all of the tungsten was incorporated into the lattice structure of the TiO_2. This indicates that the solution combustion approach developed in this study provides a simple and effective method for the doping of certain species of atoms into a TiO_2 lattice. Interestingly, it was observed that concomitant with the increasing W doping level, the (1 0 1) peak broadens and its intensity decreases. This may be attributed to the inhibition of crystal growth that is prompted by the metal dopant, which results in the formation of smaller particles [25]. The principal characteristic peak (1 0 1) for the anatase phase, located at 25.5°, was studied and used in the determination of the average crystalline size of the samples using the Scherrer equation $d = k\lambda/\beta\cos\theta$, where λ is the X-ray wavelength, β is the full width at half maximum of the (1 0 1)

Table 1
Textural properties of the samples determined by BET and XRD studies.

Sample	Surface Area ($m^2\ g^{-1}$)	Pore size (nm)	Pore volume (cm^3/g)	Crystallite size (nm)
TiO_2	52	3.6	0.220	18.80
TiO_2:N	122	3.6	0.235	11.68
TiO_2:N–W(0.5%)	128	3.7	0.260	11.82
TiO_2:N–W(1%)	147	3.6	0.290	10.34
TiO_2:N–W(1.5%)	146	4.5	0.305	10.74
TiO_2:N–W(2%)	136	4.6	0.311	9.62
TiO_2:N–W(3%)	137	6.0	0.352	9.00

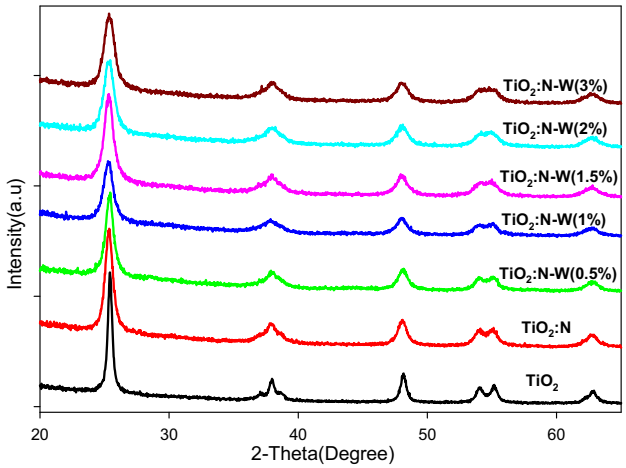

Fig. 1. XRD patterns of TiO_2, TiO_2:N and the TiO_2:N–W(*x*%).

peak, θ is the incident angle, and k is a shape factor. The calculated crystalline dimensions of the samples are shown in Table 1. It can be seen that the particle size decreases from 18.80 nm of TiO_2 to 9.00 nm of 3 at% of W doped TiO_2.

3.2. TEM observation

The as-synthesized samples were characterized by TEM. Fig. 2a and b depicts the TEM micrographs of the N-doped and N,W(1%) co-doped samples, respectively. Both of the samples show a mesoporous structure with irregular pore sizes. The insets in Fig. 2a and b are corresponding selected area electron diffraction (SAED) patterns, indicating that the two samples are polycrystalline with an anatase nature. The d value for the observed rings (0.351, 0.237, 0.189 and 0.169 nm) in both of the SAED patterns corresponds to the reflections of (1 0 1), (0 0 4), (2 0 0) and (1 0 5). Fig. 2c and d present the corresponding high resolution TEM (HRTEM) images of N-doped and N,W co-doped TiO_2, respectively. It can be seen that single crystalline TiO_2 particle with 5–8 nm size, which are in concordance with the XRD determination, interconnect with each other to form a porous network. The lattice spacing of the TiO_2

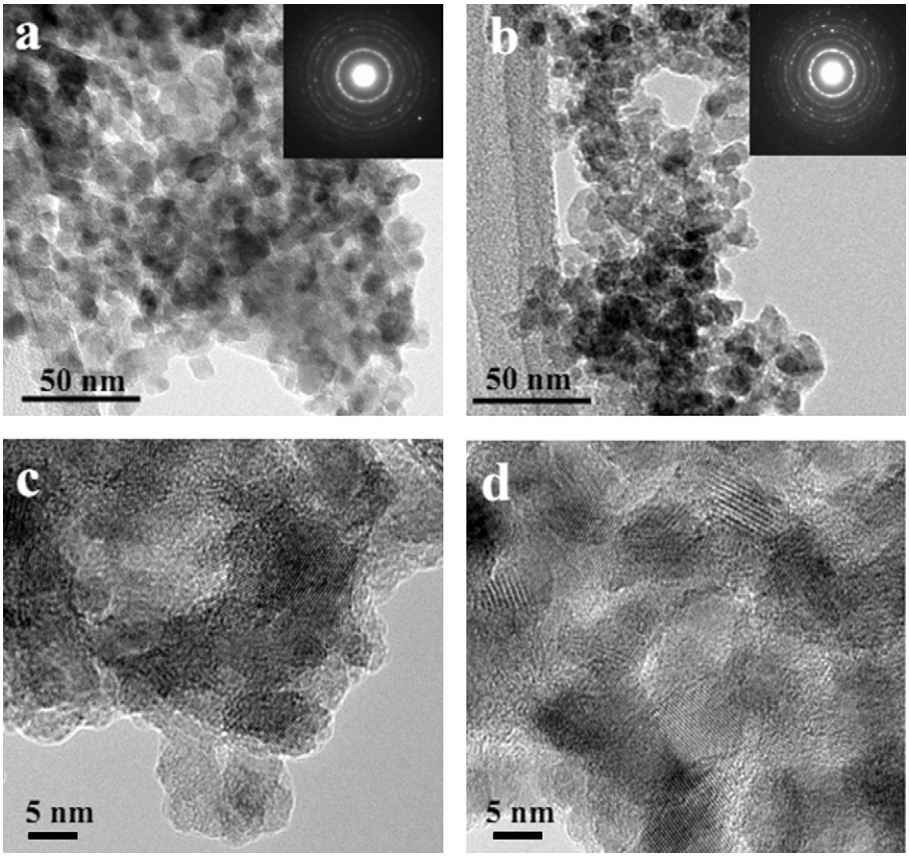

Fig. 2. TEM and high resolution TEM images of N doped (a and c) and N,W codoped TiO_2 (b and d), respectively. Inset is respective SAED pattern.

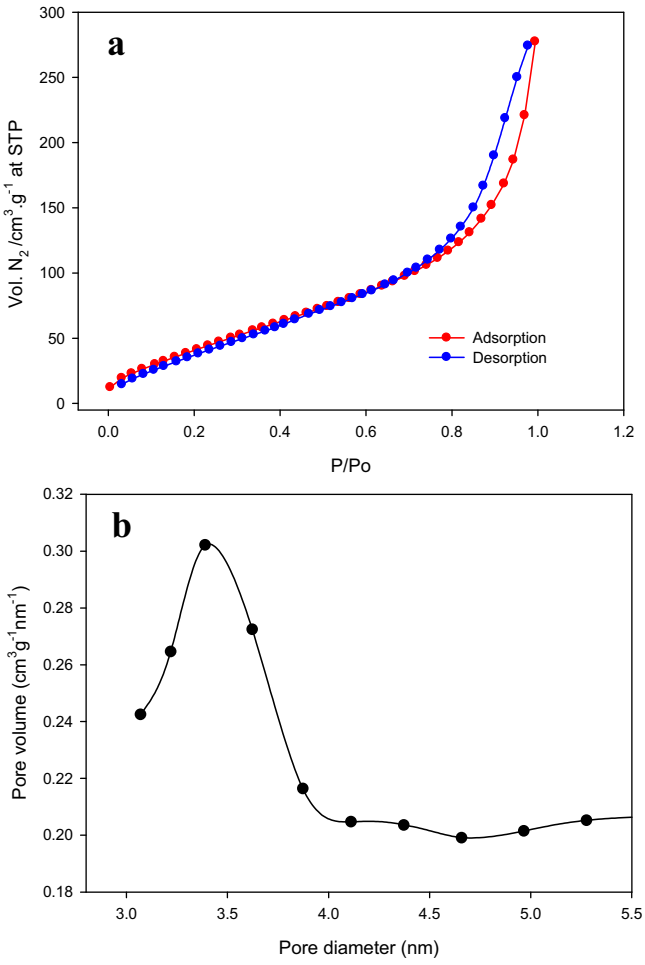

Fig. 3. (a) Nitrogen adsorption–desorption isotherms of the TiO_2:N–W(1.5%) sample, (b) Pore size distribution.

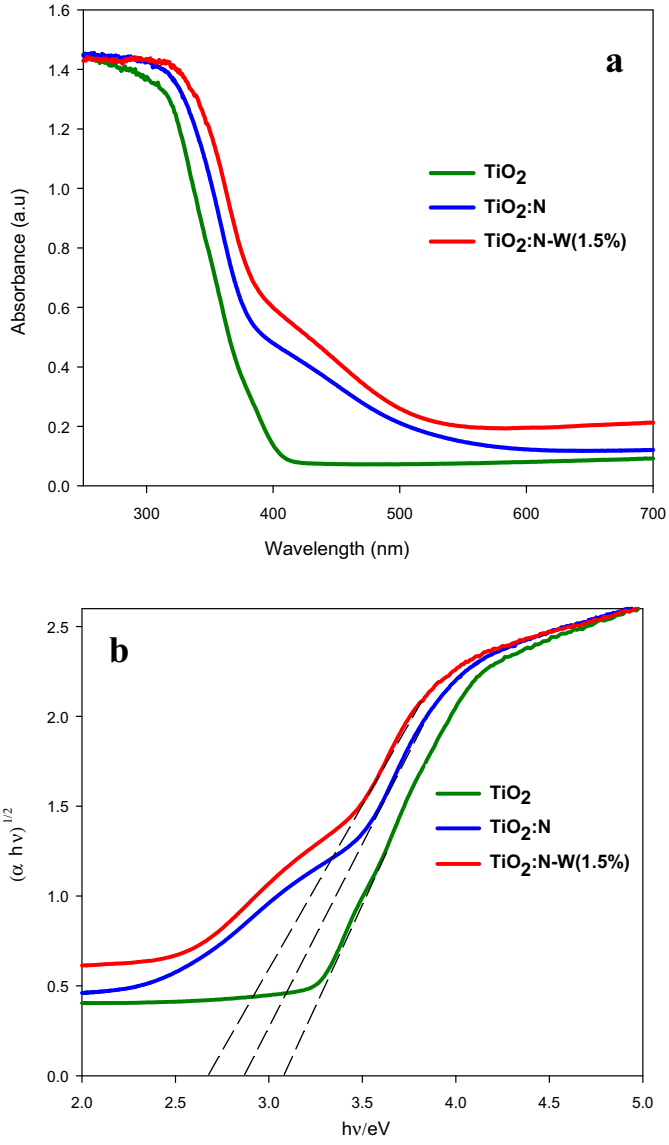

Fig. 4. (a) UV–vis absorption spectra of TiO_2, TiO_2–N and the TiO_2:N–W(1.5%); (b) Tauc plots of TiO_2, TiO_2:N and TiO_2:N–W(1.5%).

in the HRTEM images was calculated to be 0.301 nm, which corresponds to the (1 0 1) crystal plane of the anatase TiO_2 structure. The pores are visible as bright spots within the darker areas, and the size distribution is relatively narrow with an average diameter of 4–6 nm for both the N-doped and N,W co-doped TiO_2 samples.

3.3. BET surface area and pore structure

To examine the surface area, as well as the pore sizes and their distribution, nitrogen adsorption/desorption analysis was performed on all synthesized samples. Each sample showed Type IV N_2 adsorption/desorption isotherms, indicating that mesoporous structures were achieved via this synthesis method; this is consistent with the TEM observations. The isotherm curve for the N,W(1.5%)–TiO_2 sample is presented in Fig. 3a. The results of the BET analysis on the pure, doped and co-doped samples are displayed in Table 1. The specific surface area calculated for the pure TiO_2 is 51 $m^2\ g^{-1}$, which is similar to the average value for Degussa P25. However, the surface area increases in correspondence with raised W doping levels. This is ascribed to the small size and mesoporosity that is present in the structure of the samples. The surface area of 1 at% W doping is 147 $m^2\ g^{-1}$, which is close to three times that of the un-doped TiO_2 synthesized in this study using the same solution combustion method. N and W co-doping has some impact on the particle size and surface area as observed by comparing the results for W doped TiO_2 from the literature [26], where the surface area for TiO_2–W(2%) is 116 $m^2\ g^{-1}$ and the particle size is 11.6 nm. With the co-doping of N and W the surface increased to 136 $m^2\ g^{-1}$ and the particle size decreases to 9.6 nm. Since photocatalytic properties are influenced by surface area and pore size, this enhancement of specific surface area in the co-doped samples signifies the presence of additional available active sites for photocatalysis. The average pore diameter for the co-doped sample shown in Fig. 3b, which was calculated from the desorption branch of the N_2 isotherms by the Barret–Jayner–Halenda (BJH) method, is ~3.5 nm, which further validates the existence of a mesoporous structure. This finding is also consistent with the HRTEM observation. The pore sizes were observed to increase slightly with higher W doping levels.

3.4. UV–vis spectroscopic studies

The optical properties of materials are very sensitive to, and are heavily influenced by their inherent microstructures and hence electronic structural changes. UV–vis absorbance experiments were carried out, and the resulting spectra are shown in Fig. 4a. It is seen that pure TiO_2 shows absorbance only in the UV region; the absorbance shifts to longer wavelengths with N doping and

Table 2
Band gap estimation for prepared nanomaterials.

Sample	Estimated band gap (eV)
TiO_2	3.08
TiO_2:N	2.88
TiO_2:N–W(0.5%)	2.82
TiO_2:N–W(1%)	2.87
TiO_2:N–W(1.5%)	2.68
TiO_2:N–W(2%)	2.67

N,W co-doping. The corresponding Tauc plots are presented in Fig. 4b. By assuming TiO_2 to be an indirect semiconductor, the band gap energy of pure TiO_2, N doped and N,W(1.5%) co-doped TiO_2 are 3.08, 2.79, and 2.64 eV, respectively. The absorbance edge in the N doped and N,W co-doped powders was significantly shifted to the visible region. Table 2 presents the calculated band gap for the samples. This red shift is attributed to the presence of nitrogen and tungsten in the lattice structure of the TiO_2. This modification serves to alter the electronic band structure.

3.5. XPS analysis

All of the samples were analyzed by XPS to investigate the chemical components, their electronic state, and atomic concentration. The XPS spectra of TiO_2–N,W(1.5%) are presented in Fig. 5. As seen in Fig. 5a, the peaks for Ti $2p_{3/2}$ and Ti $2p_{1/2}$ are centered at 458.69 and 464.38 eV. This clearly shows the presence of a Ti (IV) oxidation state in all samples. The O1s XPS spectra shown in Fig. 5b reveal a well-defined peak at 530.01 eV with a small shoulder centered at 531.52 eV. The peak at 530 eV is characteristic of the oxides of transition metals. The small peak centered at 531.52 eV could be attributed to the presence of hydroxyl groups or adsorbed water molecules on the surface [27].

A controversy still exists as to which peak corresponds to the doped N in the TiO_2. Asahi et al. and other researchers assign the

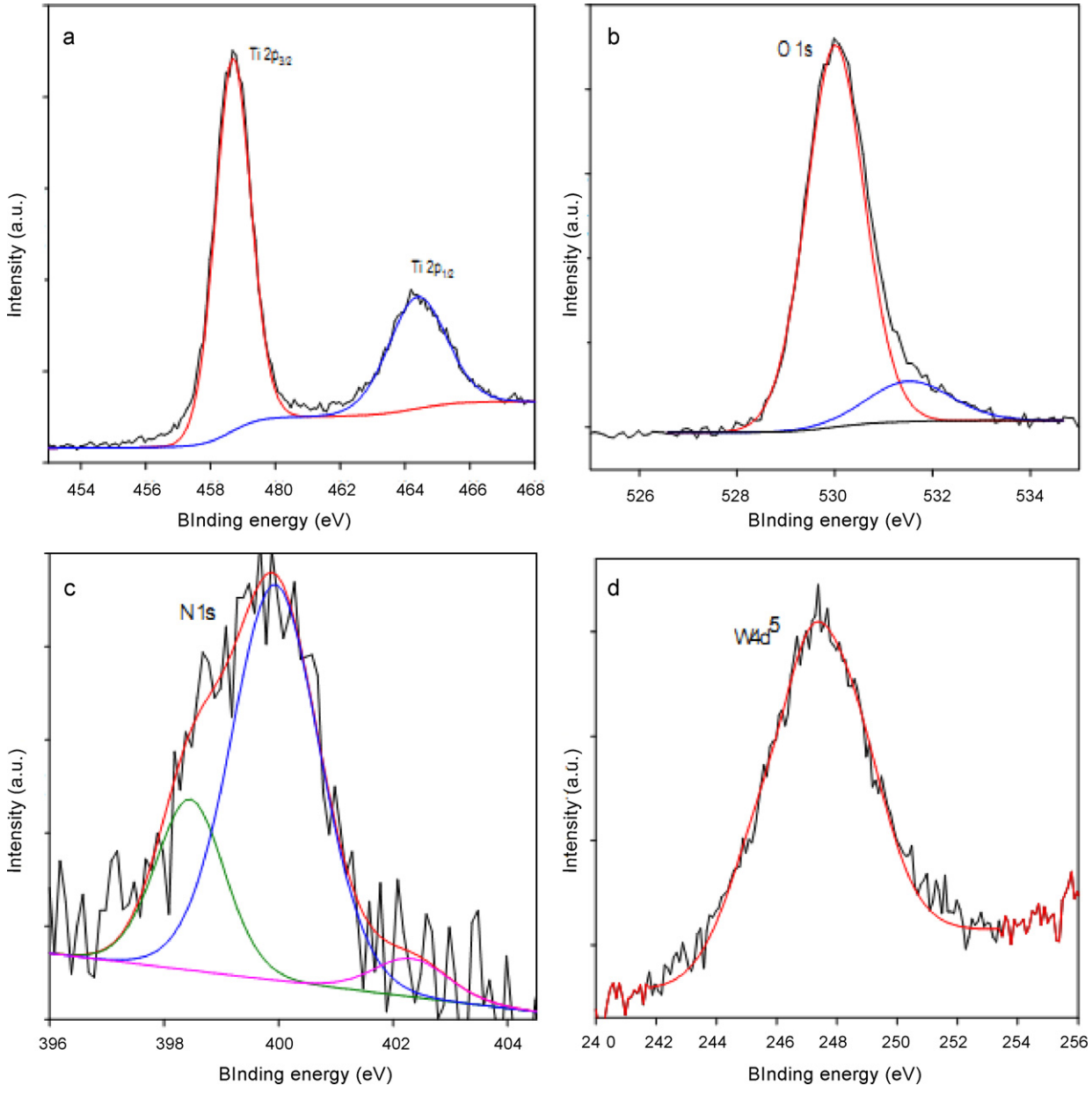

Fig. 5. XPS spectra of (a) Ti 2p, (b) O1s, (c) N1s and (d) W $4d^5$ for TiO_2:N–W(1.5%).

Table 3
Chemical constitution of the samples determined by XPS.

Sample	At wt% of N	At wt% of W
TiO_2	n/a	n/a
TiO_2:N	0.61	n/a
TiO_2:N–W(0.5%)	0.62	0.56
TiO_2:N–W(1%)	0.58	1.11
TiO_2:N–W(1.5%)	0.57	1.68
TiO_2:N–W(2%)	0.40	2.07
TiO_2:N–W(3%)	0.66	2.78

peak at 397 eV to anionic doping in which O atoms are substituted by N atoms, and the peak at 399 eV and 402 eV to the molecularly chemisorbed N [14,28]. This is altercated by Sato et al., who postulates that the peak at 399 eV is due to the interstitial doping of N into the crystal structure of TiO_2 and not chemisorption; an interpretation that is supported by many others [29–32]. Contrary to the above results some authors have attributed the peak at 399 eV to substitution nitrogen doping [33,34]. As shown in Fig. 5c, a broad peak extending from 397.5 to 402.5 eV is observed for all the N containing samples. These were fitted via a curve-fitting procedure to give three very distinct peaks centered at 397.93, 399.79 and 402.72 eV. The peaks at 397.93 eV and 399.79 eV may be assigned to substitutional doping in the form of N–Ti–O and interstitial doping as Ti–N–O, respectively. The peak located above 400 eV might be attributed to chemisorbed N containing compounds [35]. For tungsten, as shown in Fig. 5d, only one strong peak at 247.06 eV is observed. This peak may be assigned to the W dopant within the TiO_2 structure as there was no WO_3 detected in the XRD studies. The value is ~0.5 eV lower than the values obtained by other researchers for the W_{4d} in W doped TiO_2 [36], indicating that the presence of N in the lattice has some significant effect on the surrounding electronic structure. The atomic percentages of nitrogen and tungsten were calculated from their respective peak areas and the results are shown in Table 3. The doping percentage level of nitrogen was almost constant as the amount of urea used in all of these experiments was the same. The tungsten doping level was also observed to be consistent with the amount of tungsten solution added during the synthesis of the samples.

3.6. Visible-light-induced catalytic activity studies

We tested our as-synthesized samples under UV light, showing that they exhibit very similar photocatalytic activity as P25. The photodegradation reaction of Rhodamine B (RhB) under visible light ($\lambda > 420$) irradiation was thus used to evaluate and compare the photocatalytic activity of un-doped, N-doped and N,W co-doped TiO_2 and commercial Degussa P25. The irradiation time was 2 h and a sample was collected from the reaction mixture at 20 min intervals to measure the absorbance of RhB using a Cary 50 UV–vis spectrometer. Calibration measurements were performed to correlate the concentration between the dynamic range of 2.5–25 μM and the absorbance of RhB, as illustrated in Fig. 6. The linear regression equation was calculated to be $A = 0.098c - 0.129$ with a correlation coefficient of 0.999. Fig. 7 presents the kinetic curves for the photodegradation of Rhodamine B over P25 and the N-doped TiO_2 and N,W co-doped TiO_2 samples. The kinetics curves for the photodegradation of the dye on the un-doped TiO_2 synthesized in this study and P25 are almost the same. In contrast, the photodegradation of the dye on the N-doped TiO_2 is much more rapid than that on P25, and the speed of degradation is further dramatically improved by increasing the amount of W dopant in the samples until 1.5 at% doping level of W was achieved. Beyond this level a continuous decrease in photocatalytic activity is observed, which indicates that there exists a maximum doping level. Based on the modeling analysis by Puma [37,38], the differences in

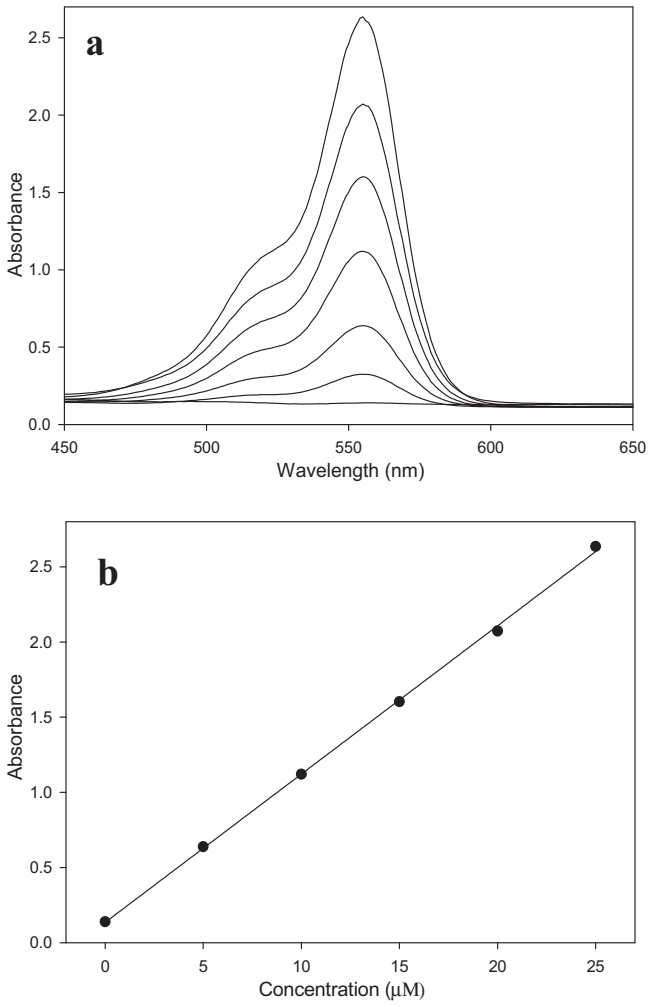

Fig. 6. (a) Calibration curve for Rhodamine B; (b) relationship between absorbance and concentration at 553 nm.

the dye degradation kinetics may be caused by different optical characteristics of each catalyst in suspension if the materials have different particle sizes. In this study, all the samples were prepared using the same method under similar conditions. As shown in Table 1, the synthesized N,W-codoped TiO_2 catalysts possess similar BET surface area and particle size. The difference observed

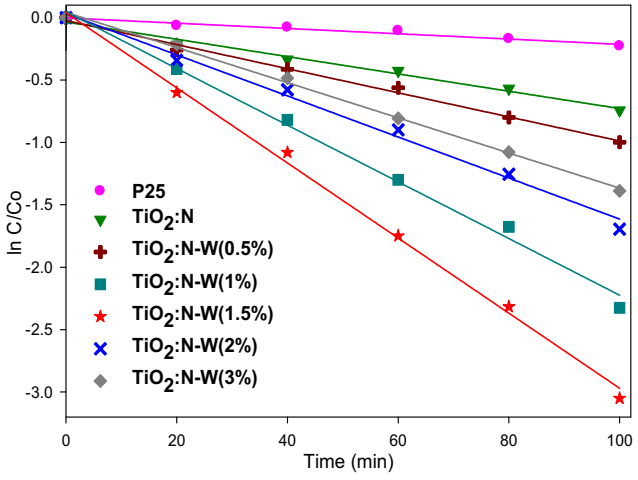

Fig. 7. Kinetic curves for the photodegradation of Rhodamine B over the TiO_2, N-doped TiO_2 and N,W co-doped TiO_2 samples.

Table 4
First order kinetic constant and relative coefficient for degradation of Rhodamine B over prepared samples.

Sample	Rate constant (min^{-1})	R^2
P25	2.12×10^{-3}	0.962
TiO_2:N	6.94×10^{-3}	0.986
TiO_2:N–W(0.5%)	9.65×10^{-3}	0.994
TiO_2:N–W(1%)	2.27×10^{-2}	0.994
TiO_2:N–W(1.5%)	3.01×10^{-2}	0.997
TiO_2:N–W(2%)	1.64×10^{-2}	0.991
TiO_2:N–W(3%)	1.40×10^{-2}	0.997

in the photocatalytic activity can be attributed to the level of the doped W. On one hand, doping can reduce the band gap energy of materials, and therefore may harvest more visible light, which is favorable for photocatalytic efficiency, whereas on the other hand, impurities that are added to the semiconductor lattice due to doping might result in the formation of defects which act as recombination centers. In this co-doping system, the physically larger atomic W occupies more volume than atomic Ti. Hence, a high doping level will produce a significant defect concentration. The detailed kinetics of the reaction is presented in Table 4. The kinetic calculations reveal that the rate of photodegradation of RhB on the TiO_2–N,W(1.5%) is approximately 14 times higher than that on the P25, demonstrating that the co-doped samples enable a significant enhancement in the visible light induced photocatalytic activity.

The photodegradation of organic dyes on the surface of a TiO_2 based photocatalyst is generally initiated by the irradiation of the reaction mixture with a light source, which excites and transitions the electrons from the valence band to the conduction band. The energy inherent to visible light is not adequate to excite an electron of pure TiO_2 due to the wide band gap of ~3.08 eV, which results in poor photocatalytic activity. The significantly enhanced visible light activity of the prepared N,W co-doped TiO_2 is explained by the fact that doping with nitrogen, which replaces the oxygen atoms resident within the TiO_2 lattice structure creates an impurity level that is just above that of the valence band. The simultaneous doping with tungsten introduces an impurity level that is just below the conduction band; thereby narrowing the band gap and leading to the augmented visible light response of these solution combustion synthesized photocatalysts. Consequently, when these co-doped TiO_2 are irradiated, the electrons may be promoted from the valence band to the impurity level introduced by the doping of the metal atom, or from the lower to higher impurity level. Subsequently, these electrons are captured by the adsorbed O_2 to give $O_2^{\bullet -}$, and the water molecules adsorbed on the surface of the catalyst react with the hole(+) vacancies to give $OH^{\bullet}$. Finally, these active oxygen species attack the dye radical cations and decompose them. The proposed sequential mechanism is as follows.

(a) Absorption of energy

$$TiO_2 + h\nu \rightarrow h^+ + e^- \quad (1)$$

(b) Generation of active oxygen species

$$O_2 + e^- \rightarrow O_2^{\bullet -} \quad (2)$$

$$H_2O + h^+ \rightarrow H^+ + OH^{\bullet} \quad (3)$$

(c) Oxidation of dye

$$RhB + O_2^{\bullet -} \rightarrow \text{products} \quad (4)$$

$$RhB + OH^{\bullet} \rightarrow \text{products} \quad (5)$$

The slight activity of pure TiO_2 as observed in Fig. 7 may be attributed to a photosensitized process whereby RhB absorbs visible light, which results in an intramolecular $\pi \rightarrow \pi^*$ transition. The photoelectrons in π^* are injected into the conduction band of the TiO_2 from where the same series of reactions ensue, as shown below.

$$RhB + h\nu \rightarrow RhB^*$$

$$RhB^* + TiO_2 \rightarrow RhB^{\bullet +} + TiO_2\,(e)$$

$$TiO_2\,(e) + O_2 \rightarrow TiO_2 + O_2^{\bullet -}$$

$$RhB^{\bullet +} + O_2^{\bullet -} \rightarrow \text{products}$$

4. Conclusions

We have successfully prepared mesoporous N-doped and N,W co-doped TiO_2 photocatalysts with an exclusive anatase phase and a high specific surface area utilizing a facile, reproducible and inexpensive solution combustion synthesis. The atomic percentage of N was kept constant, whereas that of W was varied. The textural, morphological and chemical composition studies with the prepared samples were done using various characterization techniques. XPS analysis showed that the N and W atoms were well incorporated into the lattice structure of the titania by this combustion preparation method, thus leading to a significant red shift in the absorption edge of the co-doped TiO_2, and concordantly, a dramatic narrowing of the band gap was observed. This narrowing of the band gap serves to induce high visible light response photocatalytic activities in the co-doped samples in comparison to those of P25 and therefore, may be beneficially utilized in green chemistry. Photodegradation studies of Rhodamine B dye on the different samples revealed that an enhancement factor of up to 14 times in the reaction rate was observed with the 1.5 at% W doped sample in contrast to commercial Degussa P25. The novel combustion process developed in this study is rapid and reproducible, and can be easily scaled-up, thus opening a door to fabricate high-performance TiO_2 photocatalysts for promising environmental applications.

Acknowledgements

This work was supported by a Discovery Grant from the Natural Sciences and Engineering Research Council of Canada (NSERC). A. Chen acknowledges NSERC and the Canada Foundation of Innovation (CFI) for the Canada Research Chair Award in Materials and Environmental Chemistry.

References

[1] W.C. Tincher, Text. Chem. Color 21 (1989) 33–35.
[2] P.K. Malik, Dyes Pigment 56 (2003) 239–249.
[3] H.B. Fu, C.S. Pan, W.Q. Yao, Y.F. Zhu, J. Phys. Chem. B 109 (2005) 22432–22439.
[4] Y.M. Xu, C.H. Langfor, Langmuir 17 (2001) 897–902.
[5] S. Horikoshi, F. Hojo, H. Hikaka, N. Serpone, Environ. Sci. Technol. 38 (2004) 2198–2208.
[6] F. Herrera, A. Lopez, G. Mascolo, P. Albers, J. Kiwi, Water Res. 35 (2001) 750–760.
[7] M. Tian, G. Wu, B. Adams, J. Wen, A. Chen, J. Phys. Chem. C 112 (2008) 825–831.
[8] G.S. Wu, T. Nishikawa, B. Ohtani, A. Chen, Chem. Mater. 19 (2007) 4530–4537.
[9] T. Sreethawong, S. Laehsalee, S. Chavadev, Catal. Commun. 10 (2009) 538–543.
[10] A. Ghicov, J.M. Macak, H. Tsuchiya, J. Kunze, V. Haeublein, L. Frey, P. Schmuki, Nano Lett. 6 (2006) 1080–1082.
[11] G.S. Wu, J.P. Wang, D.F. Thomas, A. Chen, Langmuir 24 (2008) 3503–3509.
[12] S.U.M. Khan, M. Al-Shahry, W.B. Ingler Jr., Science 297 (2002) 2243–2245.
[13] T. Ihara, M. Miyoshi, Y. Iriyama, O. Matsumoto, S. Sugihara, Appl. Catal. B. Environ. 42 (2003) 403–409.
[14] R. Asahi, T. Washizuka, N. Yoshino, K. Aoki, Y. Taga, Science 293 (2001) 269–271.
[15] Y.F. Ma, J.L. Zhang, B.Z. Tian, F. Chen, L.Z. Wang, J. Hazard. Mater. 182 (2010) 386–393.
[16] G. Wu, J. Wen, J. Wang, D.F. Thomas, A. Chen, Mater. Lett. 64 (2010) 1728–1731.
[17] T. Lindgren, J.M. Mwabora, E.D. Avendano Soto, J. Jonsson, A. Hoel, C.G. Granqvist, S.-E. Lindquist, J. Phys. Chem. B 107 (2003) 5709–5716.
[18] K.X. Song, J.H. Zhou, J.C. Bao, Y.Y. Feng, J. Am. Ceram. Soc. 91 (2008) 1369–1371.
[19] E.A. Reyes-Garcia, Y.P. Sun, D. Raftery, J. Phys. Chem. C 111 (2007) 17146–21715.

[20] A. Kubacka, B.B. Baeza, G. Colon, M.F. Garcia, Appl. Catal. B. Environ. 93 (2010) 274–281.
[21] A. Kubacka, G. Colon, M.F. Garcia, Appl. Catal. B. Environ. 95 (2010) 238–244.
[22] J. Li, J. Xu, W.L. Dai, H. Li, K. Fan, Appl. Catal. B. Environ. 82 (2008) 233–243.
[23] Y.F. Shen, T.Y. Xiong, T.F. Li, K. Yang, Appl. Catal. B. Environ. 83 (2008) 177–185.
[24] B. Gao, Y. Ma, Y. Cao, W. Yang, J. Yao, J. Phys. Chem. B 110 (2006) 14391–14397.
[25] Y. Zhang, A. Reller, J. Mater. Chem. 11 (2001) 2537–2541.
[26] A. Kubacka, G. Colon, M.F. Garcia, Catal. Today 143 (2009) 286–292.
[27] J.A. Rengifo-Herrera, E. Mielczarski, N.C. Castillo, J. Kiwi, C. Pulgarin, Appl. Catal. B. Environ. 84 (2008) 448–456.
[28] N.C. Saha, H.G. Tompkins, J. Appl. Phys. 72 (1992) 3072.
[29] S. Sato, R. Nakamura, S. Abe, Appl. Catal. A. Gen. 284 (2005) 131–137.
[30] Y. Wang, C.X. Feng, M. Zhang, J.J. Yang, Z.J. Zhang, Appl. Catal. B. Environ. 104 (2011) 268–274.
[31] O. Diwald, T.L. Thompson, E.G. Goralski, S.D. Walck, J.T. Yates, J. Phys. Chem. B 108 (2004) 52–57.
[32] G.S. Wu, J. Wen, S. Nigro, A. Chen, Nanotechnology 21 (2010) 085701–085706.
[33] H.X. Li, J.X. Li, Y.I. Huo, J. Phys. Chem. B 110 (2006) 1559–1565.
[34] H. Irie, Y. Watanabe, K. Hashimoto, J. Phys. Chem. B 107 (2004) 5483–5486.
[35] X. Yang, C. Cao, L. Erickson, K. Hohn, R. Maghirang, K. Klabunde, Appl. Catal. B. Environ. 91 (2009) 657–666.
[36] A. Kubacka, M.F. Garcia, G. Colon, J. Catal. 254 (2008) 272–284.
[37] G.L. Puma, A. Brucato, Catal. Today 122 (2007) 78–90.
[38] G.L. Puma, Environ. Sci. Technol. 37 (2003) 5783–5791.